JCBFM

Cerebral arterial pulsatility is linked to hippocampal microvascular function and episodic memory in healthy older adults

Tomas Vikner[1] (ID), Anders Eklund[1,2], Nina Karalija[1,2] (ID),
Jan Malm[3], Katrine Riklund[1,2] (ID), Ulman Lindenberger[4,5,6],
Lars Bäckman[7], Lars Nyberg[1,2,8] and Anders Wåhlin[1,2]

Abstract

Microvascular damage in the hippocampus is emerging as a central cause of cognitive decline and dementia in aging. This could be a consequence of age-related decreases in vascular elasticity, exposing hippocampal capillaries to excessive cardiac-related pulsatile flow that disrupts the blood-brain barrier and the neurovascular unit. Previous studies have found altered intracranial hemodynamics in cognitive impairment and dementia, as well as negative associations between pulsatility and hippocampal volume. However, evidence linking features of the cerebral arterial flow waveform to hippocampal function is lacking. We used a high-resolution 4D flow MRI approach to estimate global representations of the time-resolved flow waveform in distal cortical arteries and in proximal arteries feeding the brain in healthy older adults. Waveform-based clustering revealed a group of individuals featuring steep systolic onset and high amplitude that had poorer hippocampus-sensitive episodic memory ($p = 0.003$), lower whole-brain perfusion ($p = 0.001$), and weaker microvascular low-frequency oscillations in the hippocampus ($p = 0.035$) and parahippocampal gyrus ($p = 0.005$), potentially indicating compromised neurovascular unit integrity. Our findings suggest that aberrant hemodynamic forces contribute to cerebral microvascular and hippocampal dysfunction in aging.

Keywords

4D flow MRI, arterial stiffness, hippocampus, cognition, vasomotion

Introduction

Hippocampal vascular dysfunction is increasingly recognized in cognitive decline and dementia, as indicated by human studies on blood-brain barrier (BBB) leakages.[1–3] The pathophysiological mechanisms could involve age-related arterial wall remodeling with concomitant increases in arterial stiffness, translating to excessive microvascular pulsatility and damage to the neurovascular unit.[4,5] Regional variability in cerebral vascularization patterns suggest that some structures, such as the hippocampus, could be particularly exposed to steep pressure gradients and pulsatile stress.[6,7] Human studies have found elevated intracranial pulsatility in individuals with mild cognitive impairment[8] (MCI) and Alzheimer's disease[9,10] (AD) as well as negative associations to hippocampal volume.[11] Further, recent longitudinal findings showed that steep systolic

[1]Department of Radiation Sciences, Umeå University, Umeå, Sweden
[2]Umeå Center for Functional Brain Imaging (UFBI), Umeå University, Umeå, Sweden
[3]Department of Clinical Science, Neurosciences, Umeå University, Umeå, Sweden
[4]Center for Lifespan Psychology, Max Planck Institute for Human Development, Berlin, Germany
[5]Max Planck, UCL Centre for Computational Psychiatry and Ageing Research, Berlin, Germany
[6]Max Planck, UCL Centre for Computational Psychiatry and Ageing Research, London, UK
[7]Ageing Research Center, Karolinska Institutet and Stockholm University, Stockholm, Sweden
[8]Department of Integrative Medical Biology (IMB), Umeå University, Umeå, Sweden

Corresponding authors:
Tomas Vikner, Department of Radiation Sciences, Umeå University, SE 901 87 Umeå, Sweden.
Email: tomas.vikner@umu.se

Anders Wåhlin, Department of Radiation Sciences, Umeå University, SE 901 87 Umeå, Sweden.
Email: anders.wahlin@umu.se

onset in carotid artery pressure and flow dynamics could predict cognitive decline.[12] These observations prompt investigating cerebral arterial hemodynamics, hippocampal microvascular function, and hippocampus-sensitive cognition in healthy individuals.

The integrity of the hippocampal complex is particularly critical for episodic memory (EM) performance.[13,14] Memory decline is a characteristic feature of aging;[15] however, pronounced hippocampal atrophy and EM dysfunction are hallmarks of AD.[16,17] Hippocampal and whole-brain microvascular function can be assessed by perfusion imaging[18] and from low-frequency oscillations (LFOs) in the blood oxygen-level dependent (BOLD) signal during rest.[19,20] Microvascular LFOs are potentially evoked by neurovascular coupling, and may play a role in cerebrospinal fluid-based clearance of metabolic waste.[21,22] Therefore, a breakdown of this mechanism may indicate damage to the neurovascular unit, and may potentially lead to accumulation of harmful substances, such as amyloid-β (Aβ) and tau.[23]

Cerebral arterial hemodynamics can be assessed by transcranial Doppler (TCD) ultrasound, but such measurements are limited to acoustic windows.[24] In contrast, velocity sensitive phase contrast (PC) MRI may access all intracranial vasculature that the sequence can resolve. In 2D PC, the imaging slices need to be specified at the vessel segments of interest prior to scan, making whole-brain investigations of complex branching patterns impractical. In 4D flow MRI (3D PC), velocities are encoded in all three spatial directions simultaneously, time-resolved over the cardiac cycle and with full brain coverage.[25–28] Previously, we have shown that by sampling and averaging flow waveforms from numerous arterial cross sections in a 4D flow MRI volume, a whole-brain representation of the cardiac related waveform can be obtained in small, distal cerebral arteries.[29]

Here, we use high-resolution 4D flow MRI to examine cerebral arterial hemodynamics in a population-based cohort of healthy older adults. Using a clustering-approach, we identify a subgroup of individuals featuring steep systolic onset and high amplitude in the arterial flow waveforms. We then investigate whether this subgroup display poorer performance in EM, working memory (WM), and perceptual speed (PS) tasks, three cognitive domains that express stable individual differences and high age sensitivity.[30] To characterize potential group differences in microvascular function, we analyze perfusion and LFOs in whole-brain grey matter and in the hippocampal complex specifically. Finally, to follow-up on the group-based analyses, we evaluate the contributions of physiological and continuous hemodynamic parameters to cognitive performance, perfusion, and LFOs.

Materials and methods

Participants

Data were obtained from the Cognition, Brain, and Aging (COBRA[31]) prospective cohort of healthy individuals (N = 181; 81 women; age 64–68 years) randomly selected from the population registry in Umeå, Sweden. Participants were screened for global cognitive disturbances by a Mini Mental State Examination (MMSE) where a score of at least 27 out of 30 was required for study inclusion. Further exclusion criteria were based on factors that could affect cognition or compromise the validity of the results, including traumatic brain injury, stroke, dementia, intellectual disability, movement disorders, epilepsy, psychiatric disorders, diabetes, certain medications, severe visual or auditory impairment, poor understanding of the Swedish language, and claustrophobia. Time-resolved 4D flow MRI data were missing for 22 participants and cognitive scores were missing for 2 participants. Thus, the study population consisted of 157 participants (69 women; age 64–68 years).

The study was conducted in accordance with the Declaration of Helsinki and approved by the Regional Ethical board of Umeå, Sweden. Written informed consent was provided from all participants prior to any testing.

Magnetic resonance imaging

MRI acquisitions were performed on all individuals using a 3 T scanner (Discovery MR 750; GE Healthcare, Milwaukee, Wisconsin) with a 32-channel head coil. These included 4D flow MRI scans for intracranial hemodynamics and pulsatility, structural T_1-weighted scans for volumetric assessment and co-registrations, arterial spin labeling (ASL) for cerebral perfusion, fluid-attenuated inversion recovery (FLAIR) for white-matter lesions (WML), and resting-state functional MRI to detect microvascular LFOs. None of the scans involved any contrast agents.

4D flow MRI. The 4D flow MRI scans were performed using a phase contrast vastly undersampled isotropic-voxel projection reconstruction (PC-VIPR) that provides whole-brain flow velocities in all three spatial directions, time-resolved over the cardiac cycle.[25,26] In addition to velocity data, a complex difference (CD) volume that highlights vascular structures was reconstructed from the 4D flow MRI scans. The following imaging parameters were used: 5-point velocity encoding (venc): 110 cm/s, TR/TE: 6.5/2.7 ms, flip angle: 8°, radial projections: 16000, temporal resolution: 20 frames per cardiac cycle, resolution at

acquisition: $300 \times 300 \times 300$, imaging volume: $22 \times 22 \times 22\,cm^3$, spatial resolution after reconstruction: $320 \times 320 \times 320$, and isotropic voxel size: 0.69 mm. Scan time was approximately 9 min. The venc (110 cm/s) was selected based on the upper bound of previous 4D flow MRI studies on cerebral arterial hemodynamics.[9,31–34] Gradient errors due to eddy currents and concomitant fields were removed using polynomial fitting to the background field.[35]

Structural MRI. T_1-weighted volumes were obtained by a 3D fast-spoiled gradient echo sequence that provides high-resolution anatomical detail of the brain. 176 slices were acquired using the following imaging parameters: TR/TE: 8.2/3.2 ms, flip angle: 12°, slice thickness: 1 mm, in-plane resolution: 0.98 mm, field of view: $25 \times 25\,cm$, and phase acceleration: 2.

Perfusion MRI. 3D pseudo-continuous arterial spin labeling (pcASL) was used to obtain whole-brain perfusion maps. The following pcASL imaging parameters were used: labeling time: 1.5 s, post-labeling delay time: 1.5 s, field of view: 24 cm, slice thickness: 4 mm, in-plane resolution: 1.88 mm, and acquisition resolution: 8×512 (arms $\times$ data points) with 3 number of averages.

Fluid attenuated inversion recovery MRI. FLAIR volumes were obtained to assess total white-matter lesion (WML) volume. 46 slices were acquired using the following imaging parameters: TR/TE: 8000/120 ms, slice thickness: 3 mm, in-plane resolution: 0.94 mm, and field of view: 24×24 cm.

Resting state functional MRI. Blood oxygen level dependent (BOLD) contrast sensitive T_2^*-weighted single-shot gradient echoplanar imaging volumes were acquired to obtain functional data during resting-state conditions. 37 slices were obtained using the following parameters: TR/TE: 2000/30 ms, flip angle: 80°, slice thickness: 3.4 mm with 0.5 mm spacing, in-plane resolution: 2.6 mm, and field of view: 25×25 cm. Prior to data collection, 10 dummy scans were performed. Data were collected during 5 min 40 s.

Cerebral arterial blood flow and pulsatility

All 4D flow MRI data processing to retrieve pulsatile flow waveforms was performed in MATLAB (R2019b, Natick, Massachusetts: The MathWorks Inc). One distal and one proximal arterial flow waveform were extracted for each individual, using previously evaluated post-processing methods that utilize flow-averaging over multiple arterial cross sections to improve velocity-to-noise levels.[29,31] To characterize the arterial flow waveforms, we considered the pulsatility index

previously used to differentiate between healthy controls, individuals with MCI[8] and individuals with AD[9,10] and rate of change during early systole, as well as waveform-based clustering to identify potential subgroups within the full sample – an exploratory approach that makes contact with previous methods by simultaneously considering all waveform-features, such as amplitude[9] and rate of change.[12]

Distal cerebral arterial waveform extraction. Distal cerebral arterial waveforms were obtained from the 4D flow data using an automatic post-processing method.[29] The CD volume was first processed using a vessel-enhancement filter to provide better visualization of small cerebral vessels.[36] The filtered CD volume was binarized using a global intensity-based threshold (2.5%), and a centerline-processing algorithm[31] was used to extract a representation of the cerebral vasculature. Time-resolved (cardiac-gated) pulsatile flow waveforms were sampled automatically from double-oblique cut-planes along the entire centerline structure using local thresholding (50%) of the filtered CD volume. The thresholds (2.5% and 50%) were not evaluated explicitly, but waveforms obtained using these thresholds agreed well with reference methods, as shown previously.[29] Distal cerebral arteries were automatically identified (Figure 1(b)) using a combination of waveform analysis to separate arteries and veins, a binary cerebral mask to exclude extracerebral vessels, and a diameter threshold to exclude vessels that were considered too large (estimated diameter >1.25 mm). In terms of anatomy, distal arteries are therefore difficult to define in detail; however, visual inspection indicated that the segmentations were dominated by cortical branches. Following the automatic identification of distal arteries, suspected veins and extracranial arteries were removed manually by inspecting maximum intensity projections of the identified arteries (together with the CD volumes) from all three directions sequentially. Finally, the flow data from all identified distal cerebral arteries were normalized and aggregated into a global, composite flow waveform.[29]

Proximal arterial waveform extraction. Proximal arterial waveforms were obtained from the 4D flow MRI data using semi-automatic post-processing.[31] Seed points were manually placed in the left and right internal carotid arteries (ICA) and in the basilar artery (BA) by inspection of the CD volumes. For each seed point, time-resolved pulsatile flow-waveforms were sampled automatically for up to 15 cut planes using local thresholding (at 20% as suggested by a previous study evaluating flow accuracy[37]) of the CD volumes (Figure 1 (a)). Due to anatomical differences between the anterior and posterior circulation, the shape of the BA
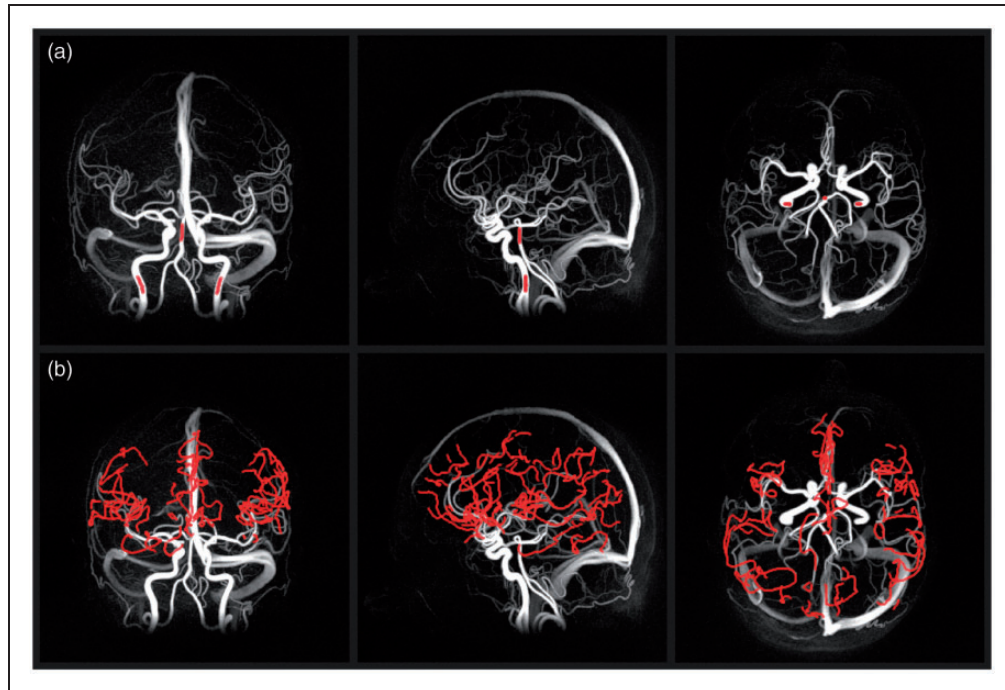
Figure 1. Maximum intensity projections of a 4 D flow MRI complex difference volume and the arterial cross sections (red) included in the analyses for an example subject. (a) Flow waveforms were obtained using semi-automatic post-processing[31] with seed points in the basilar artery (BA) and internal carotid arteries (ICAs). The proximal pulsatile flow waveform (Figure 3(a)) was computed as the average of the ICA waveforms, while the BA waveform was included only to assess total cerebral blood flow. (b) Distal flow waveforms were obtained by aggregating data from numerous arterial cross sections that were separated from extracranial arteries, large arteries (estimated diameter >1.25 mm) and veins, using a previously developed post-processing method.[29]

waveform is expected to be different than the ICA waveforms. Hence, the flow data from the two ICA waveforms were averaged into a composite, proximal flow waveform to assess hemodynamics, whereas the BA waveform was included to assess total cerebral blood flow only.

Waveform and pulsatility analyses. Following the post-processing steps to retrieve the composite (distal and proximal) flow waveforms, all individual waveforms were normalized (through division by mean flow rate), interpolated from 20 to 2000 frames per cardiac cycle using cubic splines, and synchronized after the systolic onset. Interpolation was necessary to achieve accurate synchronization of the individual waveforms, as cardiac-phase differences (related to gating) can be further minimized with higher temporal resolution. To characterize the flow waveforms, we considered both continuous and categorical variables. Waveform-based clustering was used to identify potential subgroups within the full sample, forming categorical variables. This was done using K-means clustering that aims to partition the individual waveforms into K clusters automatically, by iteratively assigning each waveform to one out of K centroid waveforms (while attempting to minimize the total within-cluster sum of squares

errors). The silhouette method (used to estimate how well the waveforms are matched to their own cluster) was used to estimate the optimal number of clusters. The pulsatility index (i.e. waveform amplitude after normalization[29]) and maximum rate of change (i.e. the highest derivative of the waveform during early systole) were considered as continuous variables to characterize the flow waveforms.

4D flow MRI derived total cerebral blood flow. Total cerebral blood flow (ml/min) was calculated from the 4D flow MRI data by adding the ICA and BA flow rate contributions, and then normalized through division by total brain volume.

Cognitive test battery

Test scores for episodic memory (EM), working memory (WM), and perceptual speed (PS) were based on a comprehensive cognitive test battery of nine tasks.[38] EM was based on word recall, number–word recall, and object–position recall; WM was based on letter updating, numerical 3-back, and spatial updating; PS was based on letter comparison, number comparison, and figure comparison. For each individual task, scores were summed over the total number of

trials, preceded by at least one practice trial. Finally, the three task scores for each cognitive domain were standardized using z-scores (i.e. mean 0; SD 1) and averaged into composite scores. Thus, each cognitive domain was represented by a single cognitive score. More detailed task descriptions are available elsewhere.[38]

Regional analyses of volumes, perfusion, and microvascular low-frequency oscillations

The hippocampus, parahippocampal gyrus (consisting of the parahippocampal and entorhinal cortices), and whole-brain grey matter (GM) were specifically selected as regions of interest (ROIs) for the region-specific analyses. The hippocampus and parahippocampal gyrus were specifically selected because of their critical roles for EM performance[13] and since BBB breakdown in these regions likely happens early in MCI[1–3].

ROI segmentation. Automatic atlas-based cortical parcellation[39] and subcortical segmentation[40] was performed using FreeSurfer 5.3 (https://surfer.nmr.mgh.harvard.edu/). The segmentations were performed on the individual T_1-weighted volumes for volumetric analyses and on a subject-averaged T_1-weighted volume for region-specific perfusion and LFO analyses. Whole-brain GM perfusion and LFOs were also computed using a sample-specific GM template in Montreal Neurological Institute (MNI) space and a 50% threshold on GM probability.

Regional brain volumes. The regional brain volumes obtained from the segmentations were normalized by the estimated total intracranial volume (eTIV) by subtracting residuals from a linear fit between the volume of interest and the eTIV.[41] The volumes were estimated as the voxel volume times the number of voxels within each ROI.

Cerebral perfusion. Whole-brain perfusion maps (ml/100g/min) were calculated from the pcASL scans using post-processing software provided by the scanner manufacturer.[18] The perfusion maps were normalized to MNI space before the analyses.

Microvascular low-frequency oscillations (LFOs). The resting-state fMRI data were preprocessed in several steps, including motion correction, slice-timing correction, and spatial normalization to MNI space. The BOLD time-series data were then averaged over brain regions of interest to increase signal-to-noise levels. From the averaged data, the fractional amplitude of low-frequency fluctuations (fALFF) was computed for each region by taking the sum of the low-frequency (0.01–0.1 Hz) amplitudes divided by the sum of all (0.01–0.25 Hz) amplitudes.[19] Since the proximity to major arteries could bias our results, the fALFF method was selected to suppress physiological noise.[19]

White matter lesions

Total WML volume was computed using the SPM12 software and a lesion-growth algorithm[42] implemented in the LST toolbox 2.0.14 (www.statisticalmodelling.de/lst.html) with combined information from T_1-weighted and FLAIR volumes as input. First, T_1-weighted volumes were segmented into tissue probability maps for gray matter, white matter, and cerebrospinal fluid. Next, FLAIR intensities were used in combination with the tissue probability maps to compute lesion maps. The lesion maps were then binarized into lesion probability maps using a pre-defined threshold ($\kappa = 0.3$) and region growing. Finally, the lesion probability maps were thresholded (50%) to acquire the individual WML volumes (cm^3).

Blood pressure and cardiovascular risk

Systolic blood pressure (SBP) and diastolic blood pressure (DBP) were measured in the left arm during sitting position. Cardiovascular risk was calculated from age, sex, SBP, treatment for hypertension, body mass index, smoking, and diabetes. The risk score was calculated based on an algorithm proposed by findings from the Framingham Heart Study, where Cox proportional-hazard regression models were used to predict the risk of developing any form of cardiovascular disease during a 10-year period.[43,44] Pulse pressure (PP) was calculated as $PP = SBP - DBP$.

Heart rate variability

Peripheral pulse oximeter data was used for heart rate variability (HRV) calculations. Total spectral power was estimated as the variance of beat-to-beat fluctuations in the heart rate. Data were analyzed by visual inspection to remove spurious ectopic beats and signal segments of insufficient quality. Cases with questionable oximeter data from the fMRI session were removed (n = 5) in analyses including HRV.

Statistical analyses

Statistical tests

Associations between the pulsatility index, rate of change and primary variables were tested with Pearson correlation. Two-sample t-tests were used to test for between-group differences between the high- and low-pulsatility groups with effect size

reported as Cohen's d. To test whether the pulsatility–EM association was reliably stronger than the pulsatility–WM and pulsatility–PS associations, the contrast among the correlated correlation coefficients was tested with a Z-test.[45] Multiple linear regression was used to residualize primary variables for potential confounders, including age, gender, years of education, and risks of developing cardiovascular diseases. Cognitive variables were further adjusted for whole-brain perfusion, and LFOs for heart rate and heart rate variability. Partial correlation was used to test for potential associations between continuous variables and the primary variables, using the same covariates. Alpha level was 0.05 for all statistical tests. No multiple comparisons correction was applied as our hypothesis was directed specifically towards hippocampus-sensitive EM and hippocampal microvascular function. Auxiliary tests were performed to characterize how pulsatility was related to other variables.

Missing data

The initial sample of 181 individuals was reduced to 157 because of missing time-resolved 4D flow MRI data (n = 22) and cognitive (n = 2) data. The following data were also missing for some individuals: years of education (n = 1), perfusion (n = 1), LFOs (n = 1), total intracranial volume (n = 1), and total WML volume (n = 4). In addition, the clustering approach excluded individuals (25/157) for the main analyses (see results section – waveform-based clustering). Thus, the study population consisted of: years of education (n = 131), perfusion (n = 131), LFOs (n = 131), regional volumes (n = 131) and WML volume (n = 128) for the main analyses, and: years of education (n = 156), perfusion (n = 156), LFOs (n = 156), regional volumes (n = 156) and WML volume (n = 153) for the supplementary analyses. Moreover, fMRI oximeter data inspection lead to additional exclusions (n = 5) for the HRV-LFO analyses, reducing the study population for the confounder-adjusted LFOs in the main analyses (n = 127) and supplementary analyses (n = 151), and for the HRV-LFO correlations (n = 151) in the supplementary analyses.

Results

Waveform-based clustering revealed subgroups of distinct arterial hemodynamic features

Waveform-based clustering (using K-means) was applied separately on the distal and proximal arterial flow waveforms (Figure 2). Both the analysis of the distal and proximal waveforms suggested the existence of two subgroups, characterized mainly by differences
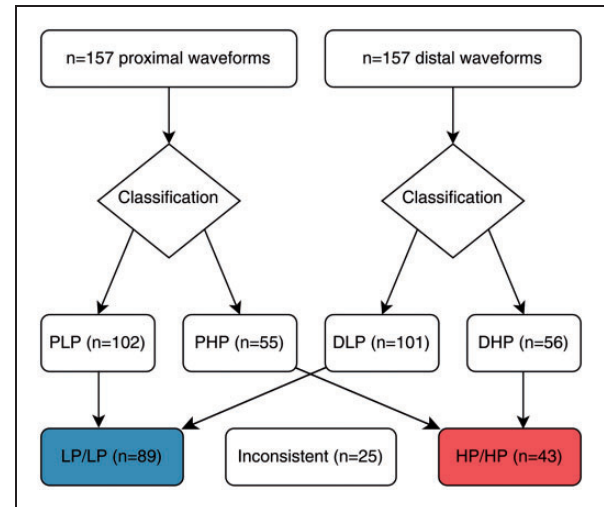

Figure 2. Waveform-based classification of the individual flow waveforms. The individual (n = 157) distal and proximal waveforms were separately analyzed with K-means clustering, forming high-pulsatility (HP) and low-pulsatility (LP) subgroups. This approach resulted in a proximal LP (PLP) subgroup (n = 102), a proximal HP (PHP) subgroup (n = 55), a distal LP (DLP) subgroup (n = 101), and a distal HP (DHP) subgroup (n = 56). The majority of individuals (n = 132) were consistently classified as LP (PLP/DLP; n = 89) or HP (PHP/DHP; n = 43), while some individuals (n = 25) were inconsistently classified as PLP/DHP (n = 13) or PHP/DLP (n = 12).

in systolic rate of change and waveform amplitude (Figure 3(a) and (b)). Based on these classifications, we formed distal and proximal high-pulsatility (HP) and low-pulsatility (LP) subgroups (Figure 2). By comparing the classifications based on distal and proximal waveforms, we found that most individuals (132/157) were consistently classified as LP (n = 89) or HP (n = 43). The rest of the sample (25/157) were classified as proximal LP–distal HP (n = 13) or proximal HP–distal LP (n = 12), but these subgroups were considered too small for statistical analyses. Demographic, cardiovascular, and waveform characteristics are provided for the consistent sample (Table 1) and for the full sample (Suppl. Table 1). The consistent subsample (n = 132) was analyzed for the main results (Figure 3) and the full sample (n = 157) was analyzed in the supplementary information (Suppl. Figure 1–2).

Hemodynamic features and cognitive performance

The associations between pulsatility and cognition were evaluated by comparing the HP and LP groups in terms of EM, WM, and PS and by linear correlation between the pulsatility index and rate of change with each cognitive variable. The group analyses revealed poorer EM performance in the HP groups, whereas weak and non-significant differences were observed
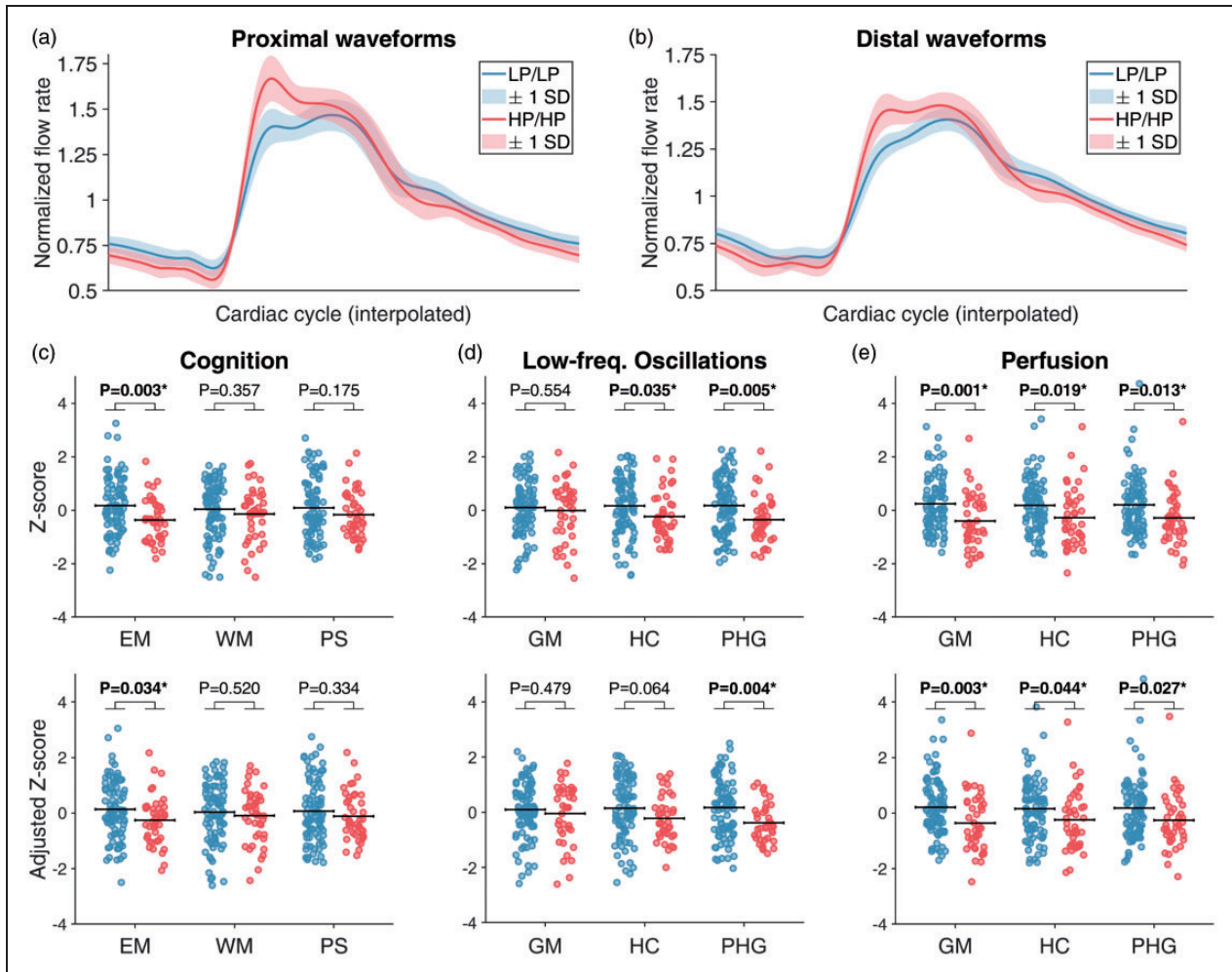
Figure 3. Cerebral arterial pulsatility in relation to cognitive performance, microvascular low-frequency oscillations (LFOs), and cerebral perfusion. (a–b) The subject-averaged proximal (a) and distal (b) arterial flow waveforms for the subsample (n = 132) of individuals classified as low-pulsatility (LP) in both proximal and distal arteries (i.e. LP/LP; blue) or high-pulsatility (HP) in both proximal and distal arteries (i.e. HP/HP; red). The shaded regions represent ± 1 standard deviation (SD). (c) Group differences between the LP/LP (blue) and HP/HP (red) subgroups in episodic memory (EM), working memory (WM) and perceptual speed (PS). (d–e) Group differences in (d) microvascular LFOs (0.01–0.1 Hz) and (e) perfusion in whole-brain gray matter (GM), hippocampus (HC) and parahippocampal gyrus (PHG). All lower panels of columns (c–e) are adjusted for age, gender, education, and cardiovascular risk by multiple linear regression. The cognitive variables (c) are further adjusted for whole-brain GM perfusion and the LFOs (d) are further adjusted for heart rate and heart rate variability. The p-values for the between-group differences were obtained from independent samples t-tests (no multiple comparisons correction).

for WM and PS (Figure 3(c)). This pattern was most prominent when considering the subsample of individuals that were consistently classified as LP (n = 89) or HP (n = 43) for both proximal and distal waveforms (Cohen's d = 0.54; Figure 3(c)), but similar associations were also observed independently for groups based on the proximal (d = 0.38) and distal (d = 0.48) waveforms (Suppl. Figure 1–2). Importantly, the group differences in EM remained significant after adjusting for potential demographic and vascular confounders, for the consistently classified sample (d = 0.39; Figure 3(c)) and for groups based on distal waveforms only (d = 0.35;

Supplemental Figure 2), but not for the proximal waveforms (p = 0.077; Supplemental Figure 1). Moreover, a Z-test indicated that the group differences in EM were stronger than the group differences in WM and PS (one-sided p = 0.036 for unadjusted data; one-sided p = 0.10 for adjusted data). Regarding the continuous variables, the pulsatility index was related to EM performance for proximal (r = −0.20, p = 0.014) but not for distal (r = −0.11, p = 0.18) waveforms, whereas rate of change was related to EM performance for both proximal (r = −0.19, p = 0.015) and distal (r = −0.20, p = 0.012) waveforms (Suppl. Table 3-4). In

Table 1. Characteristics of the high (HP/HP) and low (LP/LP) pulsatility groups (n = 132/157).

	LP/LP (n = 89)	HP/HP (n = 43)	p-value
Demographic factors			
Age (years)	66 (1.2)	66 (1.3)	0.76
Gender (M, F)	45, 44	28, 15	0.35
Education (years)	13.3 (3.7)	12.7 (2.9)	0.32
Cardiovascular factors			
Systolic blood pressure (mmHg)	142 (18)	142 (15)	0.93
Diastolic blood pressure (mmHg)	87 (10)	80 (8.3)	<0.001
Pulse pressure (mmHg)	55 (13)	61 (15)	0.009
Cardiovascular risk[a]	23 (11)	27 (11)	0.08
Heart rate (beats/min)	66 (9.7)	71 (11)	0.003
Heart rate variability (beats/min)	3.2 (0.50)	3.1 (0.48)	0.33
4D flow MRI waveform dynamics			
Proximal pulsatility index[†]	0.91 (0.10)	1.15 (0.13)	<0.001
Distal pulsatility index[†]	0.82 (0.08)	0.95 (0.10)	<0.001
Proximal rate of change[‡]	0.55 (0.12)	0.81 (0.13)	<0.001
Distal rate of change[‡]	0.37 (0.07)	0.52 (0.08)	<0.001
Proximal rate of change[§]	12.0 (2.91)	19.1 (3.88)	<0.001
Distal rate of change[§]	7.99 (1.88)	12.3 (2.58)	<0.001

Note: LP/LP and HP/HP indicates classification as either low-pulsatility (LP) or high-pulsatility (HP) in both distal and proximal arteries. [a]Cardiovascular risk corresponds to estimated 10-year risk (%) of having a major cardiovascular event[43,44]. [†]Amplitude of the normalized flow waveform. [‡]Maximal derivative of the normalized waveform in terms of amplitude-change/frame (20 frames per cardiac cycle). [§]Maximal derivative of the normalized waveform in terms of amplitude-change/sec (i.e. change/frame multiplied by heart rate). The tabulated data are reported as mean (SD). The p-values for the between-group differences were obtained from independent samples t-tests (no multiple comparisons correction).

confounder-adjusted models, the proximal pulsatility index was borderline-significant (r = −0.16, p = 0.050), whereas the rate of change associations were attenuated for both proximal (r = −0.12, p = 0.15) and distal (r = −0.12, p = 0.14) waveforms (Suppl. Table 5).

Whole-brain and hippocampal differences in microvascular function and structural integrity

Following the observed group differences in EM performance, we evaluated potential differences in perfusion and LFOs in whole-brain grey matter and in the hippocampal complex specifically. We found that the HP group displayed weaker LFO amplitudes[19] in the hippocampus and parahippocampal gyrus (Figure 3(d)); two regions critical for EM performance[13] with compromised neurovascular integrity in MCI[1–3]. Further analyses revealed that heart rate (HR) and HR variability (HRV) were also related to LFOs (Suppl. Table 6), suggesting extracerebral contributions. However, when controlling the group differences for confounders (including HR and HRV), significant and borderline-significant associations could still be observed (Figure 3(d)). Moreover, the HP group displayed lower perfusion in whole-brain grey matter (GM), but this trend was slightly weaker in the hippocampus (Figure 3(e)). No differences in regional brain volumes were found between the LP and HP groups for any investigated region (Table 2). Furthermore, group differences were found for total volume of white matter lesions (WML), but these associations were non-significant after controlling for potential confounders (Table 2).

Discussion

We examined potential links between cerebral arterial pulsatility, cognition, and cerebral microvascular function in cognitively healthy older adults by grouping individuals based on features of the arterial flow waveforms. This approach revealed a subgroup of individuals with steep systolic onset and high amplitude (Figure 3(a) and (b); Table 1) that had poorer hippocampus-sensitive EM performance, independent of potential confounders, whereas the other cognitive domains showed no significant differences (Figure 3 (c)). Our findings support the notion that the microvasculature of the hippocampal complex is particularly susceptible to pulsatile stress and is affected early in aging.[7] However, previous studies on aortic stiffness have reported impairment in additional cognitive domains, suggesting that our pulsatility–cognition associations eventually will spread.[46] One explanation for our pulsatility–EM association could be that our EM score relies on the ability to memorize pairs

Table 2. Brain structure of the high (HP/HP) and low (LP/LP) pulsatility groups (n = 132/157).

Volume (ml)	LP/LP (n = 89)	HP/HP (n = 43)	p-value
Total brain volume	1114 (94)	1111 (94)	0.86
Hippocampus volume	8.12 (0.78)	7.98 (0.85)	0.33
Parahippocampal gyrus volume	8.02 (1.05)	7.86 (0.99)	0.40
White matter lesion (WML) volume	2.15 (2.44)	3.45 (3.42)	0.014
Adjusted WML volume[a]	2.26 (2.39)	3.16 (3.36)	0.083

Note: LP/LP and HP/HP indicates classification as either low-pulsatility (LP) or high-pulsatility (HP) in both distal and proximal arteries.
[a]Controlled for age, gender, education, cardiovascular risk, and whole-brain grey matter perfusion. The tabulated data are reported as mean (SD). The p-values for the between-group differences were obtained from independent samples t-tests (no multiple comparisons correction).

(e.g. object–position recall). This type of associative encoding is considered highly hippocampus-dependent.[47] Elevated pulsatility[9,10] and EM dysfunction[17] are also observed in MCI and early AD. Therefore, early interventions to reduce arterial stiffness and pulsatility (e.g. physical exercise[48] and vasodilators[49]) may improve cognitive trajectories in normal aging as well as reduce the risk of dementia.

Regional analyses of microvascular function revealed weaker LFOs in the hippocampal complex (Figure 3(d)) and lower whole-brain perfusion (Figure 3(e)) in the HP group. These results align with findings of decreased hippocampal LFOs in amnestic MCI[20] and altered LFOs in AD progression.[50,51] However, the observed LFOs may reflect a combination of neuronal activity, neurovascular coupling[21,22] and fluctuations of extracerebral origin, related to breathing- and cardiac-variability.[52] Importantly, after controlling for confounders (including HR and HRV), group differences in LFOs remained significant and borderline-significant for the parahippocampal gyrus and hippocampus, suggesting that the observed LFO differences (Figure 3(d)) partially reflect impaired microvascular function in the hippocampal complex. Regarding the perfusion associations, previous studies have linked aortic stiffness to global perfusion[53] and pulse pressure to hippocampal perfusion.[54] However, the interaction between pulsatility and perfusion may be bi-directional. Whether pulsatility-induced microvascular damage leads to hypoperfusion, or whether reduced perfusion through other mechanisms alters the flow waveforms, is difficult to determine. Importantly, the association to EM was independent of perfusion (Figure 3(c)), highlighting the importance of studying dynamic information in the flow waveforms. These findings suggest that elevated pulsatility, attenuated LFO amplitudes, and reduced perfusion are early vascular changes in a chain of deteriorating events in the aging brain.

Vascular dementia (VaD) and AD often share a mixed pathology.[55] Moreover, the severity of cognitive dysfunction in VaD and AD is closely linked to structural degeneration.[56,57] The hemodynamic waveforms in our study were not related to grey matter structure, and the link to WML volume was attenuated when controlling for potential confounders (Table 2). Associations between arterial stiffness, pulsatility, and WML burden are common findings in previous studies.[24,46,58] The weak pulsatility–WML associations in our study are therefore surprising, but may reflect that we adjusted for other vascular parameters, including perfusion (Table 2). The non-significant associations between pulsatility and hippocampal volume could be due to the relatively young age of our sample and that pulsatility-related atrophy[11] may not yet be observed. Importantly, hippocampal blood-brain barrier (BBB) breakdown has been observed in cognitively impaired individuals and has shown predictive of cognitive decline, independent of Aβ, tau, and hippocampal volume.[2,3] Furthermore, a large study on AD progression showed that cerebrovascular abnormalities precede Aβ, tau, and structural degeneration, highlighting the importance of linking vascular mechanisms to brain function in early aging.[50]

The cardiovascular mechanisms underlying the observed waveform shapes are difficult to assess. Pulse pressure was higher in the HP subgroup, but this association was mainly due to lower diastolic and not higher systolic pressure (Table 1). This finding was unexpected, considering the well-known associations between aortic stiffness and hypertension[59] and suggests that excessive pulsatility, rather than hypertension, contributes to the causal link in our study. The HP waveforms rise immediately towards maximum flow rate during systole, whereas the LP waveforms start rapidly but continues smoothly until systolic peak flow rate is reached (Figure 3(a) and (b)). This indicates that the cardiac-related waveforms provide useful data in addition to amplitude, and may explain why rate of change but not the pulsatility index was related to EM performance for the distal waveforms (Suppl. Table 4). The pronounced group differences in early systole (Figure 3(a) and (b)) could reflect underlying differences in central[60] and cerebral[33]

arterial stiffness, with implications on wave reflections and compliance, and in microvascular resistance as suggested by the marked perfusion differences (Figure 3(e)).

The high susceptibility of the hippocampal complex to pulsatile stress may stem from characteristics of vascular supply. Most cortical regions are supplied by long and tortuous arteries, providing significant pressure drops before the microcirculation is exposed.[6] In contrast, the hippocampus is vascularized by short branches arising immediately from major arteries[61] – indicating large pressure gradients and little damping-capacity.[6] Vascularization patterns were recently shown to be important for hippocampal morphology and cognitive performance.[62] Due to limitations in 4D flow MRI spatial resolution and velocity encoding sensitivity, examination of hippocampal vascularization patterns[61,62] or hippocampus-specific pulsatility measurements were not possible in our study. Our proximal arteries provide pulsatility measurements proximal to the hippocampal branches, whereas our distal measurements correspond to cortical arteries mainly. Therefore, despite that the distal measurements represent smaller arteries, both measurements provide global representations of the cerebral arterial waveform, potentially explaining why subgroups derived from distal and proximal measurements yielded similar results with regards to cognitive parameters (Suppl. Figure 1–2, Suppl. Table 3–5).

The inconsistent classifications (Figure 2) included one group of proximal LP–distal HP (n = 13) and one group of proximal HP–distal LP (n = 12) individuals. This could reflect differences in cerebral arterial damping-capacity[63–65] and waveform-based clustering operating on slightly different features of the distal and proximal waveforms. Venous contamination of the distal waveforms and individual differences in cerebrovascular structure could also bias the classifications; however, suspected venous segments were removed by manual inspection, and the number of distal arterial cross sections did not differ between groups (Suppl. Table 2). Importantly, while the main results (Figure 3) do not generalize to the population after excluding the inconsistent classifications, group differences in EM were also significant in separate analyses of the distal and proximal waveforms (Suppl. Figure 1–2) that included the full (n = 157) sample.

A limitation of the current cross-sectional study is its inability to establish causality. *In vitro* simulated capillary-like conditions suggest that excessive shear stress and pulsatility disrupts endothelial tight junctions and increases BBB permeability.[66,67] Therefore, human studies should combine measures of pulsatility, BBB permeability, and cognition in longitudinal settings to move towards a more precise understanding

of pulsatility as a potential trigger of microvascular damage and cognitive decline. Other limitations concern the LFOs. Breathing variations and neuronal activity were not modelled for, and whether LFOs play a relevant role for brain function is not understood. Neurovascular coupling drives microvascular and cerebrospinal fluid oscillations during sleep, and may function as a clearance mechanism for the brain.[21] However, whether attenuated LFOs during wakeful rest indicates impaired clearance is not known.

In conclusion, excessive cerebral arterial pulsatility was related to poorer EM performance, weaker LFOs in the hippocampal complex, and lower whole-brain perfusion in healthy older individuals, independent of demographic and cardiovascular confounders. We propose that altered cerebral arterial hemodynamics and cerebral microvascular dysfunction are early detrimental events in normal aging, and that hippocampus-sensitive EM shows early pulsatility-related deterioration. Aberrant hemodynamic forces may contribute to cerebral microvascular damage and accelerate progression towards cognitive impairment. Hence, early interventions to maintain normal cerebral hemodynamics may contribute to preserved neurocognitive health.

Authors' contributions

K.R., U.L., L.B. and L.N designed and acquired funding for the COBRA project. A.W. conceptualized and acquired funding for developing the cerebral blood flow

References

1. Montagne A, Barnes SR, Sweeney MD, et al. Blood-Brain barrier breakdown in the aging human hippocampus. *Neuron* 2015; 85: 296–302.
2. Nation DA, Sweeney MD, Montagne A, et al. Blood–brain barrier breakdown is an early biomarker of human cognitive dysfunction. *Nat Med* 2019; 25: 270–276.
3. Montagne A, Nation DA, Sagare AP, et al. APOE4 leads to blood–brain barrier dysfunction predicting cognitive decline. *Nature* 2020; 581: 71–76.
4. De Montgolfier O, Pinçon A, Pouliot P, et al. High systolic blood pressure induces cerebral microvascular endothelial dysfunction, neurovascular unit damage, and cognitive decline in mice. *Hypertension* 2019; 73: 217–228.
5. Muhire G, Iulita MF, Vallerand D, et al. Arterial stiffness due to carotid calcification disrupts cerebral blood flow regulation and leads to cognitive deficits. *J Am Heart Assoc* 2019; 8: e011630.
6. Spence JD. Blood pressure gradients in the brain: their importance to understanding pathogenesis of cerebral small vessel disease. *Brain Sci* 2019; 9: 21.
7. Wåhlin A and Nyberg L. At the heart of cognitive functioning in aging. *Trends Cogn Sci* 2019; 23: 717–720.
8. Pahlavian SH, Wang X, Ma S, et al. Cerebroarterial pulsatility and resistivity indices are associated with cognitive impairment and white matter hyperintensity in elderly subjects: a phase-contrast MRI study. *J Cereb Blood Flow Metab* 2020; 0271678X20927101.
9. Rivera-Rivera LA, Turski P, Johnson KM, et al. 4D flow MRI for intracranial hemodynamics assessment in Alzheimer's disease. *J Cereb Blood Flow Metab* 2016; 36: 1718–1730.
10. Rivera-Rivera LA, Schubert T, Turski P, et al. Changes in intracranial venous blood flow and pulsatility in Alzheimer's disease: a 4D flow MRI study. *J Cereb Blood Flow Metab* 2017; 37: 2149–2158.
11. Wåhlin A, Ambarki K, Birgander R, et al. Intracranial pulsatility is associated with regional brain volume in elderly individuals. *Neurobiol Aging* 2014; 35: 365–372.
12. Chiesa ST, Masi S, Shipley MJ, et al. Carotid artery wave intensity in mid-to late-life predicts cognitive decline: the Whitehall II study. *Eur Heart J* 2019; 40: 2300–2309.
13. Dickerson BC and Eichenbaum H. The episodic memory system: neurocircuitry and disorders. *Neuropsychopharmacology* 2010; 35: 86–104.
14. Gorbach T, Pudas S, Lundquist A, et al. Longitudinal association between hippocampus atrophy and episodic-memory decline. *Neurobiol Aging* 2017; 51: 167–176.
15. Rönnlund M, Nyberg L, Bäckman L, et al. Stability, growth, and decline in adult life span development of declarative memory: cross-sectional and longitudinal data from a population-based study. *Psychol Aging* 2005; 20: 3–18.
16. Jack CRJ, Petersen RC, Xu YC, et al. Prediction of AD with MRI-based hippocampal volume in mild cognitive impairment. *Neurology* 1999; 52: 1397–1403.
17. Bäckman L, Small BJ and Fratiglioni L. Stability of the preclinical episodic memory deficit in Alzheimer's disease. *Brain* 2001; 124: 96–102.
18. Alsop DC, Detre JA, Golay X, et al. Recommended implementation of arterial spin-labeled perfusion MRI for clinical applications: a consensus of the ISMRM perfusion study group and the European consortium for ASL in dementia. *Magn Reson Med* 2015; 73: 102–116.
19. Zou QH, Zhu CZ, Yang Y, et al. An improved approach to detection of amplitude of low-frequency fluctuation (ALFF) for resting-state fMRI: fractional ALFF. *J Neurosci Methods* 2008; 172: 137–141.
20. Han Y, Wang J, Zhao Z, et al. Frequency-dependent changes in the amplitude of low-frequency fluctuations in amnestic mild cognitive impairment: a resting-state fMRI study. *Neuroimage* 2011; 55: 287–295.
21. Fultz NE, Bonmassar G, Setsompop K, et al. Coupled electrophysiological, hemodynamic, and cerebrospinal fluid oscillations in human sleep. *Science* 2019; 366: 628–631.
22. van Veluw SJ, Hou SS, Calvo-Rodriguez M, et al. Vasomotion as a driving force for paravascular clearance in the awake mouse brain. *Neuron* 2020; 105: 549–561.e5.
23. Tarasoff-Conway JM, Carare RO, Osorio RS, et al. Clearance systems in the brain - Implications for Alzheimer disease. *Nat Rev Neurol* 2015; 11: 457–470.
24. Webb AJS, Simoni M, Mazzucco S, et al. Increased cerebral arterial pulsatility in patients with leukoaraiosis: arterial stiffness enhances transmission of aortic pulsatility. *Stroke* 2012; 43: 2631–2636.
25. Gu T, Korosec FR, Block WF, et al. PC VIPR: a high-speed 3D phase-contrast method for flow quantification and high-resolution angiography. *AJNR Am J Neuroradiol* 2005; 26: 743–749.
26. Johnson KM and Markl M. Improved SNR in phase contrast velocimetry with five-point balanced flow encoding. *Magn Reson Med* 2010; 63: 349–355.
27. Markl M, Frydrychowicz A, Kozerke S, et al. 4D flow MRI. *J Magn Reson Imaging* 2012; 36: 1015–1036.
28. Morgan AG, Thrippleton MJ, Wardlaw JM, et al. 4D flow MRI for non-invasive measurement of blood flow

in the brain: a systematic review. *J Cereb Blood Flow Metab* 2020; 0271678X20952014.

29. Vikner T, Nyberg L, Holmgren M, et al. Characterizing pulsatility in distal cerebral arteries using 4D flow MRI. *J Cereb Blood Flow Metab* 2020; 40: 2429–2440.

30. Verhaeghen P and Salthouse TA. Meta-analyses of age-cognition relations in adulthood: estimates of linear and nonlinear age effects and structural models. *Psychol Bull* 1997; 122: 231–249.

31. Schrauben E, Ambarki K, Spaak E, et al. Fast 4D flow MRI intracranial segmentation and quantification in tortuous arteries. *J Magn Reson Imaging* 2015; 42: 1458–1464.

32. Wen B, Tian S, Cheng J, et al. Test–retest multisite reproducibility of neurovascular 4D flow MRI. *J Magn Reson Imaging* 2019; 49: 1543–1552.

33. Rivera-Rivera LA, Cody KA, Eisenmenger L, et al. Assessment of vascular stiffness in the internal carotid artery proximal to the carotid canal in Alzheimer's disease using pulse wave velocity from low rank reconstructed 4D flow MRI. *J Cereb Blood Flow Metab* 2020; 10.1177/0271678X20910302.

34. Wåhlin A, Ambarki K, Birgander R, et al. Measuring pulsatile flow in cerebral arteries using 4D phase-contrast MR imaging. *AJNR Am J Neuroradiol* 2013; 34: 1740–1745.

35. Bernstein MA, Zhou XJ, Polzin JA, et al. Concomitant gradient terms in phase contrast MR: analysis and correction. *Magn Reson Med* 1998; 39: 300–308.

36. Jerman T, Pernus F, Likar B, et al. Enhancement of vascular structures in 3D and 2D angiographic images. *IEEE Trans Med Imaging* 2016; 35: 2107–2118.

37. Dunås T, Holmgren M, Wåhlin A, et al. Accuracy of blood flow assessment in cerebral arteries with 4D flow MRI: evaluation with three segmentation methods. *J Magn Reson Imaging* 2019; 50: 511–518.

38. Nevalainen N, Riklund K, Andersson M, et al. COBRA: a prospective multimodal imaging study of dopamine, brain structure and function, and cognition. *Brain Res* 2015; 1612: 83–103.

39. Fischl B, van der Kouwe A, Destrieux C, et al. Automatically parcellating the human cerebral cortex. *Cereb Cortex* 2004; 14: 11–22.

40. Fischl B, Salat DH, Busa E, et al. Whole brain segmentation: automated labeling of neuroanatomical structures in the human brain. *Neuron* 2002; 33: 341–355.

41. Hansen TI, Brezova V, Eikenes L, et al. How does the accuracy of intracranial volume measurements affect normalized brain volumes? sample size estimates based on 966 subjects from the HUNT MRI cohort. *AJNR Am J Neuroradiol* 2015; 36: 1450–1456.

42. Schmidt P, Gaser C, Arsic M, et al. An automated tool for detection of FLAIR-hyperintense white-matter lesions in multiple sclerosis. *Neuroimage* 2012; 59: 3774–3783.

43. D'Agostino RB, Vasan RS, Pencina MJ, et al. General cardiovascular risk profile for use in primary care: the Framingham heart study. *Circulation* 2008; 117: 743–753.

44. Karalija N, Wåhlin A, Ek J, et al. Cardiovascular factors are related to dopamine integrity and cognition in aging. *Ann Clin Transl Neurol* 2019; 6: 2291–2303.

45. Meng X-l, Rosenthal R and Rubin DB. Comparing correlated correlation coefficients. *Psychol Bull* 1992; 111: 172–175.

46. Singer J, Trollor JN, Baune BT, et al. Arterial stiffness, the brain and cognition: a systematic review. *Ageing Res Rev* 2014; 15: 16–27.

47. Sperling R, Chua E, Cocchiarella A, et al. Putting names to faces: successful encoding of associative memories activates the anterior hippocampal formation. *Neuroimage* 2003; 20: 1400–1410.

48. Kim HK, Hwang CL, Yoo JK, et al. All-Extremity exercise training improves arterial stiffness in older adults. *Med Sci Sports Exerc* 2017; 49: 1404–1411.

49. Webb AJS. Effects of vasodilating medications on cerebral haemodynamics in health and disease: systematic review and meta-analysis. *J Hypertens* 2019; 37: 1119–1125.

50. Iturria-Medina Y, Sotero RC, Toussaint PJ, et al. Alzheimer's Disease Neuroimaging Initiative. Early role of vascular dysregulation on late-onset Alzheimer's disease based on multifactorial data-driven analysis. *Nat Commun* 2016; 7: 11934.

51. Rivera-Rivera LA, Cody KA, Rutkowski D, et al. Intracranial vascular flow oscillations in Alzheimer's disease from 4D flow MRI. *NeuroImage Clin* 2020; 28: 102379.

52. Tong Y, Hocke LM and Frederick BB. Low frequency systemic hemodynamic 'noise' in resting state BOLD fMRI: characteristics, causes, implications, mitigation strategies, and applications. *Front Neurosci* 2019; 13: 787.

53. Jefferson AL, Cambronero FE, Liu D, et al. Higher aortic stiffness is related to lower cerebral blood flow and preserved cerebrovascular reactivity in older adults. *Circulation* 2018; 138: 1951–1962.

54. Laosiripisan J, Haley AP and Tanaka H. Steady state vs. Pulsatile blood pressure component and regional cerebral perfusion. *Am J Hypertens* 2017; 30: 1100–1105.

55. Schneider JA, Arvanitakis Z, Bang W, et al. Mixed brain pathologies account for most dementia cases in community-dwelling older persons. *Neurology* 2007; 69: 2197–2204.

56. Dichgans M and Leys D. Vascular cognitive impairment. *Circ Res* 2017; 120: 573–591.

57. Jack CR, Knopman DS, Jagust WJ, et al. Tracking pathophysiological processes in alzheimer's disease: an updated hypothetical model of dynamic biomarkers. *Lancet Neurol* 2013; 12: 207–216.

58. Birnefeld J, Wåhlin A, Eklund A, et al. Cerebral arterial pulsatility is associated with features of small vessel disease in patients with acute stroke and TIA: a 4D flow MRI study. *J Neurol* 2020; 267: 721–730.

59. Kaess BM, Rong J, Larson MG, et al. Aortic stiffness, blood pressure progression, and incident hypertension. *JAMA J Am Med Assoc* 2012; 308: 875–881.

60. Mitchell GF, Van Buchem MA, Sigurdsson S, et al. Arterial stiffness, pressure and flow pulsatility and brain structure and function: the age, gene/environment Susceptibility-Reykjavik study. *Brain* 2011; 134: 3398–3407.

61. Spallazzi M, Dobisch L, Becke A, et al. Hippocampal vascularization patterns: a high-resolution 7 tesla time-

of-flight magnetic resonance angiography study. *NeuroImage Clin* 2019; 21: 101609.

62. Perosa V, Priester A, Ziegler G, et al. Hippocampal vascular reserve associated with cognitive performance and hippocampal volume. *Brain* 2020; 143: 622–634.

63. Vrselja Z, Brkic H, Mrdenovic S, et al. Function of circle of Willis. *J Cereb Blood Flow Metab* 2014; 34: 578–584.

64. Zarrinkoob L, Ambarki K, Wåhlin A, et al. Aging alters the dampening of pulsatile blood flow in cerebral arteries. *J Cereb Blood Flow Metab* 2016; 36: 1519–1527.

65. Holmgren M, Wåhlin A, Dunås T, et al. Assessment of cerebral blood flow pulsatility and cerebral arterial compliance with 4D flow MRI. *J Magn Reson Imaging* 2020; 51: 1516–1525.

66. Garcia-Polite F, Martorell J, Del Rey-Puech P, et al. Pulsatility and high shear stress deteriorate barrier phenotype in brain microvascular endothelium. *J Cereb Blood Flow Metab* 2017; 37: 2614–2625.

67. Bouhrira N, Deore BJ, Sazer DW, et al. Disturbed flow disrupts the blood-brain barrier in a 3D bifurcation model. *Biofabrication* 2020; 12: 025020.